NUCL SCI TECH (2017) 28:17
DOI 10.1007/s41365-016-0168-5

Theoretical study of magnetic lens with parallel beam matched

Guo-Jun Yang[1,2] · Zhuo Zhang[1,2] · Tao Wei[1,2] · Yi-Ding Li[1,2] · Xiao-Ding Zhang[1,2] · Jin-Shui Shi[1,2]

Received: 10 August 2015 / Revised: 9 May 2016 / Accepted: 12 May 2016 / Published online: 24 December 2016

Abstract The magnetic lens (Zumbro lens) is a critical part in proton radiography. Traditionally the matched beam for Zumbro lens in proton radiography is a virtual point source beam, which is not suitable for some cases, such as cylindrical samples. In these cases, a parallel beam is more appropriate. In this paper, a method, which uses quadrupole beamline, is proposed for designing a magnetic lens with parallel beam matched. Theoretical analysis is given. The results show that the matched beam for this lens is indeed parallel beam, while the major merits of Zumbro lens are inherited. Following this method, a theoretical design based on the 11-MeV cyclotron is presented.

Keywords Proton radiography · Magnetic lens · Chromatic blur · Parallel beam · Match

1 Introduction

Charged particles, such as proton, are useful tools for transmission radiography [1–3]. Nuclear interaction with the nucleus, multiple Coulomb scattering (MCS) with the Coulomb field of the nucleus, and ionization with the electrons are three major types of interaction when protons pass through materials. However, MCS effect may seriously blur the final image. Zumbro lens (magnetic lens) can focus the scattered particles to obtain clear image, which has been successfully demonstrated both by simulations and experiments [4–17].

To eliminate the major part of chromatic blur, a matched beam of a Zumbro lens is a virtual point source beam, but this will introduce additional blur when the sample is cylindrical. In this case, a parallel beam is more appropriate.

A method for designing a magnetic lens with parallel beam matched is developed in this paper.

2 Description of Zumbro lens

A typical Zumbro lens consists of four quadrupole magnets, as shown schematically in Fig. 1, where k and l are strength and length of quadrupoles, respectively; D_1 and D_2 are the drift space lengths; and f is the focal length.

Under certain condition [4], the transfer matrix of a Zumbro lens becomes a minus identity ($-\boldsymbol{I}$) matrix, which satisfies the requirements of point-to-point imaging, being assumed for a monoenergetic incident particle beam. However, energy spread always exists, and particles off the design momentum will deviate from the central trajectory due to the chromatic aberration. This problem can be partially solved by the second-order chromatic matching.

Suppose an incident particle comes from a virtual point source at a distance L upstream of the entry plane of the lens, due to both MCS in the object and the beam emittance, the particle will exit the object at an angle

This work was supported by National Natural Science Foundation of China (Nos. 11475157, 11405162, 11205144 and 11176001), CAEP Developing Foundation (No. 2014A0402016), CAEP President Foundation (No. 201402086), and CAEP Key Laboratory Foundation (No. PPL2013PZ09).

✉ Guo-Jun Yang
baita00@aliyun.com

1 Institute of Fluid Physics, Chinese Academy of Engineering Physics, Mianyang 621900, China

2 Key Laboratory of Pulsed Power, Chinese Academy of Engineering Physics, Mianyang 621900, China

$$x_0' = wx_0 + \varphi, \quad (1)$$

where $w = L^{-1}$ is the beam correlation coefficient and φ is the angular deviation from the ideal position-angle correlation line. The matrix elements in general are functions of the fractional momentum deviation $\Delta(\equiv \delta p/p)$. By expanding the final position of the particle in Taylor series form to the first order, it is found that w should satisfy the following equations in order to realize the second-order chromatic matching design (primes indicate momentum derivatives)

$$\boldsymbol{R}_{11}' + w\boldsymbol{R}_{12}' = 0, \quad (2)$$

where $\boldsymbol{R}'_{11}$ and $\boldsymbol{R}'_{12}$ are the differentials of $\boldsymbol{R}_{11}$ and $\boldsymbol{R}_{22}$. All positions depend on chromatic aberrations vanishing, and the final transverse position is then given by

$$x = -x_0 + \boldsymbol{R}_{12}'\varphi\Delta. \quad (3)$$

The chromatic blur caused by the energy spread becomes $\boldsymbol{R}'_{12}\varphi\Delta$, and the chromatic coefficient is $\boldsymbol{R}'_{12}$.

At the mid-plane of a chromatically matched identity lens, the transverse position of a particle is given by

$$x_{\text{mid}} = \boldsymbol{M}_{12}\varphi, \quad (4)$$

where $\boldsymbol{M}$ is the transfer matrix of the first half of Zumbro lens. Equation (4) implies that after the first cell, the transverse position of the particle depends only on φ.

According to Eq. (2), the two correlation coefficients at X-plane and Y-plane can be written as follows

$$w_x = -\boldsymbol{R}_{11}'/\boldsymbol{R}_{12}', \quad (5)$$

$$w_y = -\boldsymbol{R}_{33}'/\boldsymbol{R}_{34}'. \quad (6)$$

In the Zumbro lens, we have $\boldsymbol{R}'_{11} = \boldsymbol{R}'_{33}$ and $\boldsymbol{R}'_{12} = \boldsymbol{R}'_{34}$ because of the symmetry; thus, one gets

$$w_x = -w_y. \quad (7)$$

This implies that the beam is convergent in one direction and divergent in the other one, as shown in Fig. 2.

Here the coefficient L is dependent on w_x or w_y, with the relationship $|w_x| = |w_y| = 1/L$.

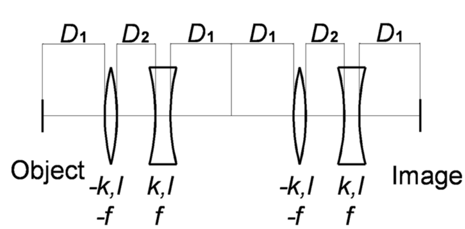

Fig. 1 Sketch of Zumbro lens

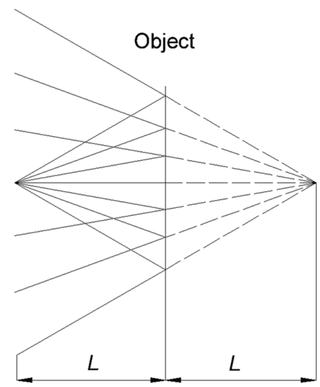

Fig. 2 Sketch of virtual point source beam for Zumbro lens

3 Demand of parallel beam radiography

Point source beam is not the best choice in some practical applications. In fact, parallel beam is much more desirable in these applications. In some radiography experiments with cylindrical samples, as shown in Fig. 3, additional blur will be introduced when a point source beam is adopted, but this can be avoided by using a parallel source beam.

Unlike the chromatic blur, the additional blur described above is interrelated with the sample, and it does not exist when there is no lateral drift in the sample. As an example, for an 800-MeV proton beam, a tentative design gives $\boldsymbol{R}'_{11} = 4.058$ and $\boldsymbol{R}'_{12} = 9.336$ m. Assume that the angular deviation of the beam is 5 mrad, and the energy deviation is 0.5%, the chromatic blur is then 0.24 mm according to Eq. (3). The correlation coefficient w_x is $-0.435\ \text{m}^{-1}$ from Eq. (5). If the cylindrical sample in Fig. 3 is sized at Φ 1 cm × 1 cm, the additional blur is 0.23 mm, which is about the same as the chromatic blur. Surely, the additional blur increases with the sample size. Parallel beam can eliminate the additional blur.

In Ref. [18], we proposed a type of magnetic lens making use of the energy-loss information of the particles. Similarly to the angle collimation in Zumbro lens, the energy can be collimated in the energy-loss lens. If both energy collimation and angle collimation are in demand,

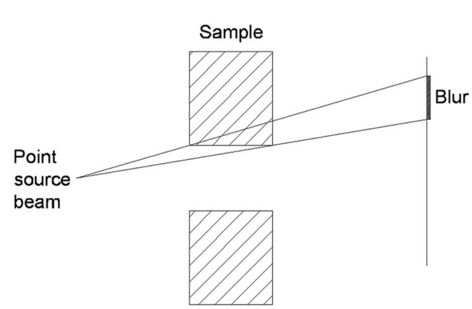

Fig. 3 Additional blur with a cylindrical sample

the energy-loss lens and Zumbro lens are expected to be cascaded, i.e., an energy-loss lens followed by a Zumbro lens, or vice versa. Unfortunately, the different matching conditions of the two types of lens prevent them from being cascaded, since the energy-loss lens demands a parallel matched beam.

So another magnetic lens with parallel beam matched is desired.

4 Design study of the new magnetic lens

Zumbro lenses have two main characteristics: (1) the transfer matrix is minus identity matrix and (2) the mid-plane is an angle Fourier plane. The new lens will inherit the two characteristics, which are two constraints for the new lens. Also, the matched beam should be parallel beam, i.e., w in Eq. (2) should be zero. So the third constraint is

$$\boldsymbol{R}'_{11} = \boldsymbol{R}'_{33} = 0. \tag{8}$$

As shown in Fig. 1, Zumbro lens forms a reflection symmetric quadrupole beamline. A quadrupole beamline is reflection symmetric if its second half is the mirror image of the first half, which means the sequence of drifts and quads is traversed in the reverse order and with the opposite signs for the magnetic fields.

The new lens has also symmetric characteristic, like Zumbro lens. Two cases are proposed here.

4.1 Reflection symmetric case

The reflection symmetry forces that [4] $\boldsymbol{R}_{44} = \boldsymbol{R}_{11}$, $\boldsymbol{R}_{33} = \boldsymbol{R}_{22}$, $\boldsymbol{R}_{34} = \boldsymbol{R}_{12}$, $\boldsymbol{R}_{43} = \boldsymbol{R}_{21}$. In this case, the lens needs at least eight quadrupole magnets to keep the symmetry characteristics. It consists of a repetition of two identical unit cells, each of which is reflection symmetric itself. The optical configuration is shown in Fig. 4, where k is the quadrupole strength, l is its length, f is its focal length, and D_1–D_3 are the drift space lengths.

Considering the symmetry, only the expressions in X-plane are analyzed in the following paragraphs. Like Zumbro lens described in Sect. 2, the transfer matrix of the whole lens is written as $\boldsymbol{R}$, and the one of the first half is written as $\boldsymbol{M}$.

The symmetry forces give that [4]

$$\boldsymbol{R} = -\boldsymbol{I} + \tau\boldsymbol{M}, \tag{9}$$

where $\tau = \boldsymbol{M}_{11} + \boldsymbol{M}_{22}$ is the trace of matrix $\boldsymbol{M}$. If the trace $\tau = 0$, it can be seen that $\boldsymbol{R}$ becomes the minus identity matrix ($-\boldsymbol{I}$), so the first constraint is satisfied.

When energy spread is included, Eq. (9) gives the momentum derivatives of the matrix elements as follows:

$$\boldsymbol{R}'_{jk} = \tau'\boldsymbol{M}_{jk}. \tag{10}$$

In particular, we get $\boldsymbol{R}'_{11} = \tau'\boldsymbol{M}_{jk}$.

Considering the third constraint of the new lens expressed in Eq. (8), since τ' is not always zero (which can be verified by a simulation of thin lens approximation), we have $\boldsymbol{M}_{11} = 0$. As the symmetry forces $\boldsymbol{M}_{11} = \boldsymbol{M}_{22}$, we have $\boldsymbol{M}_{11} = \boldsymbol{M}_{22} = 0$. At the middle plane of the lens, the particle position is $x_{\mathrm{mid}} = \boldsymbol{M}_{11}x_0 + \boldsymbol{M}_{12}x'_0$, which becomes

$$x_{\mathrm{mid}} = \boldsymbol{M}_{12}x'_0. \tag{11}$$

So the second constraint is satisfied naturally. Notice that in Eq. (4), the angle is expressed as φ, which is only the additive part in Eq. (1), while in Eq. (11), the angle is the total one in Eq. (1). However, when parallel beam is adopted, $x_0{}'$ becomes φ since w becomes zero. So on the X-plane, $\boldsymbol{M}_{11} = \boldsymbol{M}_{22} = 0$ is the only constraint required for the new lens. Conditions on the Y-plane can be got similarly, we have $\boldsymbol{M}_{33} = \boldsymbol{M}_{44} = 0$.

Since the first half is reflection symmetric, $\boldsymbol{M}_{11} = \boldsymbol{M}_{22} = 0$ and $\boldsymbol{M}_{33} = \boldsymbol{M}_{44} = 0$ are satisfied simultaneously. Equation (10) shows that $\boldsymbol{R}'_{12} = \boldsymbol{R}'_{34}$. This implies that the chromatic coefficients of X-plane and Y-plane are equal.

4.2 Symmetric case

The difference between a symmetric quadrupole beamline and a reflection symmetric one is that the magnetic fields of the second half are in opposite signs. The symmetry forces that $\boldsymbol{R}_{22} = \boldsymbol{R}_{11}$, $\boldsymbol{R}_{44} = \boldsymbol{R}_{33}$. In this case, six quadrupole magnets are enough. The configuration is shown in Fig. 5.

The deduction in Sect. 4.1 is still valid, but $\boldsymbol{M}_{11} = \boldsymbol{M}_{22} = 0$ and $\boldsymbol{M}_{33} = \boldsymbol{M}_{44} = 0$ are not definitely satisfied simultaneously since the symmetry is different.

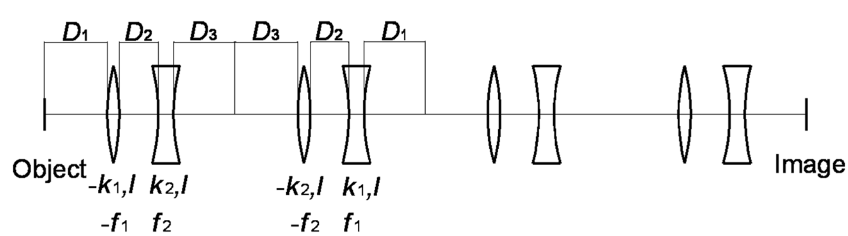

Fig. 4 Configuration of the refelction symmetric lens

Also, the chromatic aberrations of X- and Y-plane are not equal since $\boldsymbol{R}'_{12} = \boldsymbol{R}'_{34}$ is invalid.

Notice that here the first half of the lens is itself symmetric. From Eq. (10) and the symmetry condition, we have $\boldsymbol{M}_{11} = \boldsymbol{M}_{22}$, so $\tau = 0$ and $\boldsymbol{M}_{11} = \boldsymbol{M}_{22} = 0$ are of equivalence. The advantage of the symmetric case is that the number of magnets is less, while the advantage of the reflection symmetric case is that the chromatic aberrations of X- and Y-plane are equal.

5 Analysis in thin lens approximation

For a thin lens, one has $\mathrm{d}f/\mathrm{d}\Delta = f$, where f is the focal length of the thin lens.

5.1 Zumbro lens

The chromatic factor for a Zumbro lens (see Fig. 1) is

$$\boldsymbol{R}'_{12} = \boldsymbol{R}'_{34} = 4(D_1 + D_2). \tag{12}$$

Therefore, to decrease the chromatic blur of a Zumbro lens, the D_1 and D_2 should be as small as possible.

5.2 Reflection symmetric case

Write the transfer matrix of Fig. 4 in thin lens approximation. Using $\mathrm{d}f/\mathrm{d}\Delta = f$, the chromatic factor can be written as

$$\begin{aligned}\boldsymbol{R}'_{12} &= \boldsymbol{R}'_{34} \\ &= 4(D_1 + 2D_2 + 2D_3) - \frac{8D_2D_3(D_1 + D_2)}{f_2^2} \\ &\quad - \frac{8D_1D_2^2D_3(D_1 + 2D_2 + 2D_3)}{f_1^2f_2^2} \\ &\quad + \frac{16D_1D_2^3D_3^2(D_1 + D_2)}{f_1^2f_2^4}.\end{aligned} \tag{13}$$

Equation (13) is rather complicated, but calculation shows that the chromatic factor is close to the length of the magnetic lens.

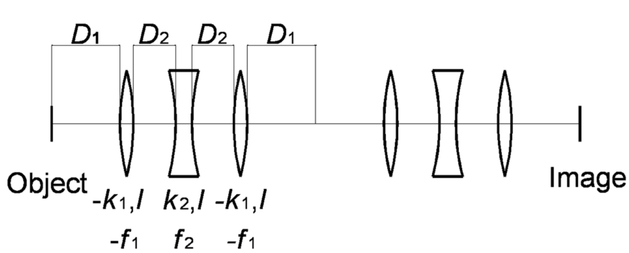

Fig. 5 Configuration of the symmetric lens

As $\boldsymbol{M}_{33} = \boldsymbol{M}_{44} = 0$, it can be deduced that f_1 and f_2 are the functions of D_1, D_2 and D_3, so does $\boldsymbol{R}'_{12}$. There are three free parameters in this system: D_1, D_2, and D_3. It is not easy to study generally. To find some quantitative laws, and for simplicity, the following three cases are considered. (a) $D_1 = nd$, $D_2 = d$, $D_3 = d$; (b) $D_1 = d$, $D_2 = nd$, $D_3 = d$; (c) $D_1 = d$, $D_2 = d$, $D_3 = nd$. Here n varies from 0 to 5. The curves in Fig. 6 can be obtained, where the values on the x- and y-axes are n and $\boldsymbol{R}'_{12}$, respectively. It can be seen that $\boldsymbol{R}'_{12}$ increases with D_1 or D_2, but decreases with increasing D_3.

5.3 Symmetric case

Write the transfer matrix of Fig. 5 in thin lens approximation. Using $\mathrm{d}f/\mathrm{d}\Delta = f$, the chromatic factors can be written as

$$\begin{aligned}\boldsymbol{R}'_{12} = -\frac{1}{f_1^4f_2^2}&2(D_2f_1 + D_1(D_2 + f_1))(f_1(D_2 - 2f_2) \\ &+ D_1(D_2 + f_1 - 2f_2)) \\ &\times \left(D_1\left(3D_2^2 + f_1(f_1 - 2f_2) + 4D_2(f_1 - f_2)\right)\right. \\ &\left.+ D_2f_1(2D_2 + f_1 - 2f_2)\right),\end{aligned} \tag{14}$$

$$\begin{aligned}\boldsymbol{R}'_{34} = -\frac{1}{f_1^4f_2^2}&2(D_2f_1 + D_1(-D_2 + f_1))(f_1(D_2 + 2f_2) \\ &+ D_1(-D_2 + f_1 - 2f_2)) \\ &\times \left(D_1\left(3D_2^2 + f_1(f_1 - 2f_2) - 4D_2(f_1 - f_2)\right)\right. \\ &\left.+ D_2f_1(-2D_2 + f_1 - 2f_2)\right)).\end{aligned} \tag{15}$$

The two factors are not equal to each other in this case. From $\boldsymbol{M}_{11} = \boldsymbol{M}_{22} = 0$ and $\boldsymbol{M}_{33} = \boldsymbol{M}_{44} = 0$, it can be deduced that f_1 and f_2 are the functions of D_1 and D_2, so do $\boldsymbol{R}'_{12}$ and $\boldsymbol{R}'_{34}$.

Again, two cases are considered: (a) $D_1 = nd$, $D_2 = d$; (b) $D_1 = d$, $D_2 = nd$. The $\boldsymbol{R}'_{12}$ and $\boldsymbol{R}'_{34}$ obtained are shown in Fig. 7. One sees that $\boldsymbol{R}'_{12}$ increases with D_1, but when D_2 increases, $\boldsymbol{R}'_{12}$ decreases first to a minimum and then increases, while $\boldsymbol{R}'_{34}$ increases with D_1, but decreases with increasing D_2.

6 Theoretical design based on 11-MeV proton beam

An 11-MeV proton cyclotron was designed and constructed at Institute of Fluid Physics [19], with CW proton beams of 11 MeV and 50 μA. The lens uses the reflection symmetric structure, with (see Fig. 4) $D_1 = 0.3$ m, $D_2 = 0.3$ m, $D_3 = 0.1$ m, $l = 0.2$ m, $k_1 = 1.89037$ T/m, $k_2 = 5.11052$ T/m, and a total length of 4.4 m.

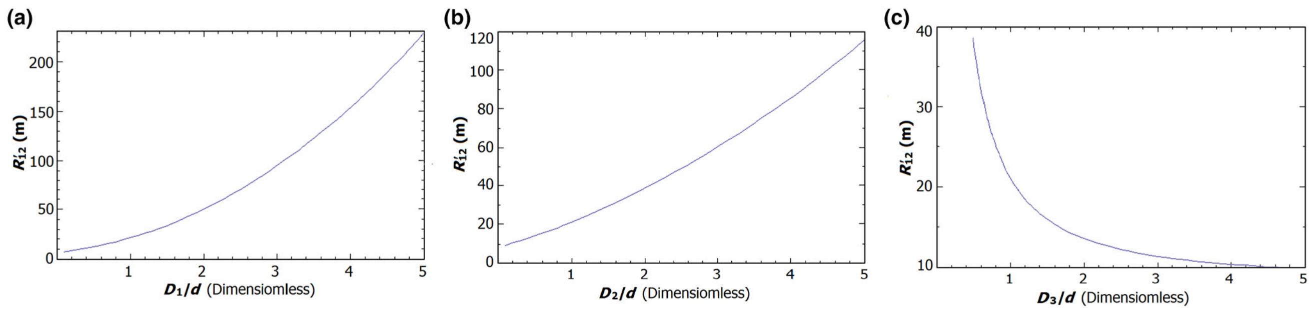

Fig. 6 Chromatic factor on three conditions

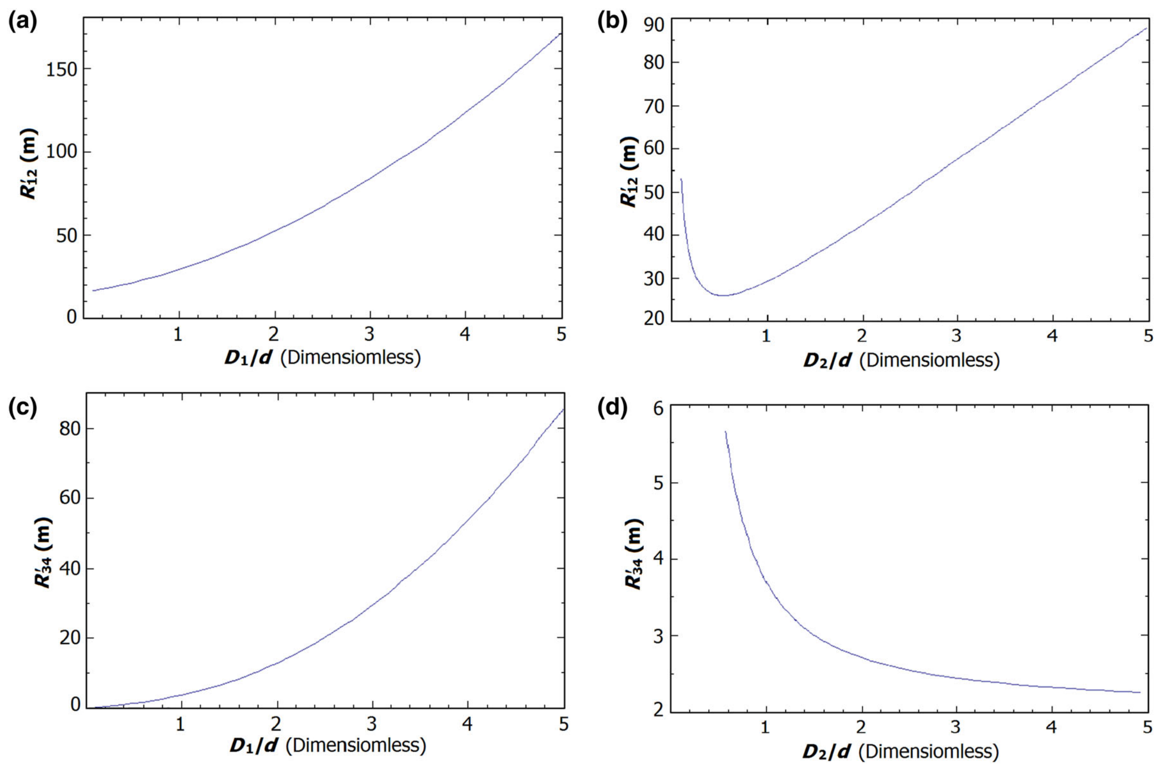

Fig. 7 Chromatic factors in X-plane (**a**, **b**) and Y-plane (**c**, **d**) on two conditions

As mentioned in Sect. 4, the chromatic coefficient $\boldsymbol{R}'_{12}$ is close to the length of the lens, which is 4.549 m.

Proton trajectories in the lens, simulated using the MyBOC code [20], are shown in Fig. 8, where different angular deviations are represented by different line styles, and Z and X are the longitude and transverse position, respectively. It can be seen that the lens is a point-to-point system. When the incident beam is parallel, particles with the same angular deviation reach the mid-plane at a same position, so the mid-plane is the angle Fourier plane. Also, the envelope oscillation is small.

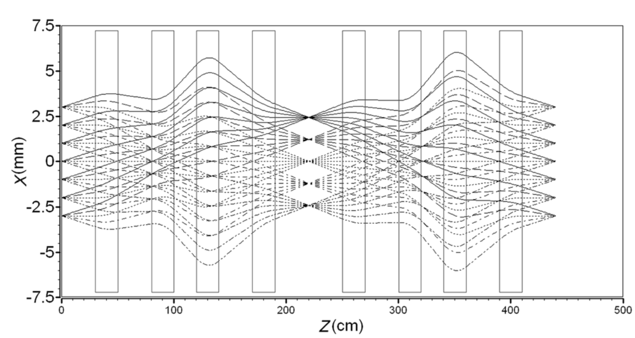

Fig. 8 Trajectories of protons

7 Conclusion

A parallel incident beam is desired in practical applications, while Zumbro magnetic lens uses virtual point source beam as its matched input. Through analyses using the transfer matrix method, we have proposed a new type of magnetic lens. It is advantageous in the matched parallel beam, while keeping the main characteristics of the Zumbro lens. Theoretical analysis, both constructions of reflective symmetry and symmetry, suggests the possible optical arrangements of the lens. The analysis shows that the new lens can fulfill all the functions of Zumbro lens. A theoretical design based on a cyclotron with 11-MeV proton beam is demonstrated. Experimental demonstration of the new imaging lens system will be carried out on this accelerator.

References

1. G.D. Hogan, K.J. Adams, K.R. Alrick, et al., Proton radiography, in *Proceedings of the 1999 particle accelerator conference*, New York, USA, March 27–April 2 (1999). doi:10.1109/PAC.1999.795765
2. C.L. Morris, N.S.P. King, K. Kwiatkowski et al., Charged particle radiography. Rep. Prog. Phys. **76**, 046301 (2013). doi:10.1088/0034-4885/76/4/046301
3. P. Ken, Particle beam radiography. Rev. Accel. Sci. Technol. **6**, 117–142 (2013). doi:10.1142/S1793626813300065
4. C.T. Mottershead, J.D. Zumbro, Magnetic optics for proton radiography, in *Proceedings of the 1997 particle accelerator conf*erence, Vancouver, BC, Canada, May 12–16 (1997). doi:10.1109/PAC.1997.750705
5. N.S.P. King, E. Ables, K.J. Adams et al., An 800-MeV proton radiography facility for dynamic experiments. Nucl. Instrum. Methods A **424**, 84–91 (1999). doi:10.1016/S0168-9002(98)01241-8
6. C.T. Mottershead, D. Barlow, B. Blind, et al., Design and operation of a proton microscope for radiography at 800 MeV, in *Proceedings of the 2003 particle accelerator conference*, Portland, Oregon, USA, May 12–16 (2003). doi:10.1109/PAC.2003.1289014
7. P.A. Rigg, C.L. Schwartz, R.S. Hixson et al., Proton radiography and accurate density measurements: a window into shock wave processe. Phys. Rev. B **77**, 220101 (2008). doi:10.1103/PhysRevB.77.220101
8. C.L. Morris, E. Ables, K.R. Alrick et al., Flash radiography with 24 GeV/c protons. J. Appl. Phys. **109**, 104905 (2011). doi:10.1063/1.3580262
9. F.E. Merrill, E. Campos, C. Espinoza et al., Magnifying lens for 800 MeV proton radiography. Rev. Sci. Instrum. **82**, 103709 (2011). doi:10.1063/1.3652974
10. L.N. Sheng, Y.T. Zhao, G.J. Yang et al., Heavy-ion radiography facility at the Institute of Modern Physics. Laser Part. Beams **32**, 651–655 (2014). doi:10.1017/S0263034614000676
11. Y. Yan, L.N. Sheng, Z.W. Huang et al., Simulation of proton radiography terminal at the Institute of Modern Physics. Laser Part. Beams **33**, 439–447 (2015). doi:10.1017/S0263034615000440
12. Y.D. Li, X.D. Zhang, T. Wei et al., Imaging principle and experiment results of an 11 MeV low-energy proton radiography system. Nucl. Sci. Tech. **25**, 060203 (2014). doi:10.13538/j.1001-8042/nst.25.060203
13. X.D. Zhang, Y.D. Li, G.J. Yang et al., Measurement of spatial resolution of 11 MeV proton radiography. Nucl. Sci. Tech. **25**, 060204 (2014). doi:10.13538/j.1001-8042/nst.25.060204
14. T. Wei, G.J. Yang, Y.D. Li et al., First experimental research in low energy proton radiography. Chin. Phys. C **38**, 087003 (2014). doi:10.1088/1674-1137/38/8/087003
15. T. Wei, G.J. Yang, J.D. Long et al., Image blur in high energy proton radiography. Chin. Phys. C **37**, 068201 (2013). doi:10.1088/1674-1137/37/6/068201
16. T. Wei, G.J. Yang, J.D. Long et al., Imaging beamline for high energy proton radiography. Chin. Phys. C **36**, 792–796 (2012). doi:10.1088/1674-1137/36/8/019
17. T. Wei, G.J. Yang, X.Z. He et al., A lattice scenario for a proton radiography accelerator. Chin Phys C **34**, 1754–1756 (2010). doi:10.1088/1674-1137/34/11/017
18. G.J. Yang, T. Wei, Z. Zhang et al., Concept and design of charged particle optics using energy Fourier plane collimation. Phys. Rev. Spec. Top. Accel. Beams **17**, 094701 (2014). doi:10.1103/PhysRevSTAB.17.094701
19. T. Wei, G.J. Yang, X.Z. He, Magnet design and test of positron emission tomography cyclotron. High Power Laser Part. Beams **24**, 2193–2197 (2012). doi:10.3788/HPLPB20122409.2193. **(in Chinese)**
20. Z. Zhang, G.J. Yang, J.Q. Lu, Lie algebraic analysis and simulation of high-current pulsed beam transport in a solenoidal lens. Chin. Phys. C **34**, 134–137 (2010). doi:10.1088/1674-1137/34/1/025